Materials Science and Engineering B 223 (2017) 143–152

Contents lists available at ScienceDirect

Materials Science and Engineering B

journal homepage: www.elsevier.com/locate/mseb

Effects of laser cutting on the structural and mechanical properties of carbon nanotube assemblages

Seyram Gbordzoe [a], Sergey Yarmolenko [b], Sathya Kanakaraj [a], Mark R. Haase [b], Noe T. Alvarez [c], Ryan Borgemenke [c], Paa Kwasi Adusei [a], Vesselin Shanov [a,c,*]

[a] Department of Mechanical and Materials Engineering, University of Cincinnati, Cincinnati, OH 45221, United States
[b] Department of Mechanical Engineering, Engineering Research Center, North Carolina A&T State University, Greensboro, NC 27411, United States
[c] Department of Biomedical, Chemical and Environmental Engineering, University of Cincinnati, Cincinnati, OH 45221, United States

ARTICLE INFO

Article history:
Received 20 March 2017
Received in revised form 18 May 2017
Accepted 16 June 2017
Available online 22 June 2017

Keywords:
Carbon nanotubes
Laser damage
Amorphous carbon
Heat-affected zone
Kerf width

ABSTRACT

Multiple applications of carbon nanotubes (CNTs) require their assembly into macroscopic materials: films, sheets, and ribbons. Most of these macro-materials are flexible thin structures and need to be cut to micrometer dimensions. Laser cutting has emerged as one of the best pressure-free alternative methods, providing accuracy and uniformity. We report on the effect of laser cutting on the structural and mechanical properties of CNT sheet assemblages. Laser cutting forms a significant and deleterious amount of amorphous carbon at and near the cut edge, and this was observed by Raman spectroscopy, transmission electron microscopy, and electron energy loss spectroscopy. The damage can have adverse effects on the physical properties of CNTs and applications based on them. Laser cutting at high power was found to reduce the tensile strength of CNT sheets by as much as 75%. Nevertheless, at smaller cut widths, the mechanical properties were affected irrespective of the laser power.

1. Introduction

Carbon nanotubes (CNTs) have been studied extensively since its wide introduction to the research community in 1991 [1–3]. CNTs are an allotrope of carbon and can be described as a graphene sheet rolled into a tube. Because of individual CNTs' unique structure, they have excellent physical properties, such as high mechanical strength (100–200 GPa), low electrical resistivity (3×10^{-5} Ω.cm), and high thermal conductivity (3500 W/m.K) [4–6]. Nevertheless, transferring these properties from the nanoscale into a macroscale material made of CNTs has proven challenging. To advance practical applications, more attention is being paid toward exploring and processing CNTs into bulk materials such as sheets and yarns [6–16] (generalized here as CNT assemblages). Often, applications of these assemblages require cutting and forming to particular dimensions. Some of the methods used for these tasks include mechanical cutting, liquid-phase oxidative cutting, solid-state reaction cutting, and electron-induced cutting [17,18]. Focused ion beam (FIB), although considered as an expensive approach, has also been used for fragmenting CNT assemblages [19–21]. However, such cutting methods have drawbacks, such as considerable material loss, lack of precision and reproducibility, high time consumption, and nonuniformity of the cut edge.

Laser cutting minimizes these drawbacks and therefore has become one of the most common methods for tailoring CNT assemblages for various applications [22–25]. The laser cut quality, described by the kerf and heat-affected zone (HAZ), is an important parameter that is usually studied. The kerf is defined as the width of the material that is removed during the laser cutting process, while the HAZ is the area around the cut edge whose properties are affected by the laser cutting. Determining the kerf width is necessary because for any cut sample, the amount of material removed will help identify the tolerance needed to achieve cut parts with precise dimensions. Ghavidel et al. studied the effect of CNT content on laser cutting of CNT/poly(methyl methacrylate) nanocomposites [26]. Their findings showed that an increase in CNT content led to a decrease in HAZ. This is because CNTs are more thermally conductive than the polymer and therefore reduced the thermal focus. Hix et al. also studied the effect of laser power and cutting speed on the kerf width. They found that an increase in laser power and cutting speed caused an increase in the kerf width [27]. The kerf width was also shown to depend on the alignment direction of the material. It was reported that the kerf width was smaller when the direction of cutting was parallel

* Corresponding author at: Department of Mechanical and Materials Engineering, University of Cincinnati, Cincinnati, OH 45221, United States.
E-mail address: vesselin.shanov@uc.edu (V. Shanov).

http://dx.doi.org/10.1016/j.mseb.2017.06.010
0921-5107/

to the fiber direction than that when the direction was perpendicular [28]. This was because the thermal conductivity is higher in the parallel direction than that in the perpendicular direction, thereby allowing heat to be propagated better. There have also been studies on how laser cutting affects the structural properties of CNTs. Tachibana examined the effects of laser-induced defects on single-wall carbon nanotubes (SWCNTs) by Raman spectroscopy and reported that the laser irradiation increased the D band intensity, and this can be attributed to the defects created in the tubes [29]. On the contrary, Cheong et al. reported that the laser trimming of CNT forests did not transform the tubes into amorphous carbon, preserving their pristine nature [30]. There is, however, very little research published on how laser cutting affects the physical properties of CNT assemblages or their composites. The publication closest to our topic describes how CO_2 laser was used to improve the electrical conductivity of CNT/poly(methyl methacrylate) composites [31].

In this paper, we present an in-depth study of the effect of laser cutting on the structural properties of CNT sheets and how the laser exposure can affect their mechanical properties. The effect of laser power on the kerf width and HAZ was examined by scanning electron microscopy (SEM) and Raman spectroscopy. The effects of laser cutting on the structural properties of CNTs were also studied by transmission electron microscopy (TEM) and electron energy loss spectroscopy (EELS). Mechanical tests were also conducted on CNT sheets cut at different laser powers.

2. Experimental methods and techniques

2.1. CNT sheet fabrication

CNTs used in this study were grown by the chemical vapor deposition (CVD) method. Iron (Fe)-based catalyst with a thickness of approximately 1.2 nm was sputtered on a 4-inch silicon (Si) wafer, which was previously coated with a 5-nm alumina (Al_2O_3) buffer layer. The coated Si wafer was loaded into a modified commercial CVD reactor ET3000 from CVD Equipment Corporation for CNT growth. Details about the growth conditions can be found elsewhere [32]. The CNTs grown by this method are vertically aligned and predominantly multiwalled with approximately 3–5 walls. The vertically aligned CNT arrays were used for preparing CNT sheets. A ribbon was drawn from one end of the array and wound onto a roller covered with Teflon film. The sheet assembling process is illustrated in Fig. 1, where each revolution of the roller produces a layer of CNT sheet. The sheets were densified by spraying acetone every 10 layers until a total of 100 layers were accumulated. Nanotubes in the sheet produced were aligned parallel to the drawing direction as shown in the inset of Fig. 1(b). The thickness of the CNT sheets was measured using a micrometer and confirmed by SEM to be 6 μm.

2.2. Laser cutting

A laser micromachining system by Oxford Lasers with an X-Y stage was used to cut CNT sheets. The device characteristics are as follows: solid-state laser with a wavelength of 532 nm, maximum pulse energy of 2 mJ, maximum average power of 4 W, frequency of 1000 Hz, resolution of 1 μm, and pulse duration of 10–500 ns. Laser cutting was performed in ambient air and pressure. The samples were cut under different powers (0.5%, 5%, and 50% of the maximum average power of 4 W) for each width at a speed of 2 mm/s and three cutting passes. The cutting speed and number of passes reported are the optimized parameters to ensure complete cutting of CNT sheets.

2.3. Characterization methods

Surface and cross-sectional morphology of CNT sheets were analyzed using an FEI XL30 SEM. The effect of laser cutting on the structural properties of CNTs was studied using an FEI image-corrected Titan3 G2 30–300 TEM. Raman spectroscopy (Horiba LabRam Aramis μ-Raman system, wavelength 532 nm, laser power: ~10 mW, grating: 600 lines/mm, and spectral resolution: ~2.8 cm^{-1}/point) was used to conduct spectral analysis of CNT sheets.

Mechanical testing of the CNT sheet samples was conducted using a uniaxial tensile testing machine (Instron 5948, maximum air pressure applied to the pneumatic grips equal to 5 Bar and maximum load equal to 100 N). The strain rate of testing was kept constant at 0.5 mm/s for all experiments

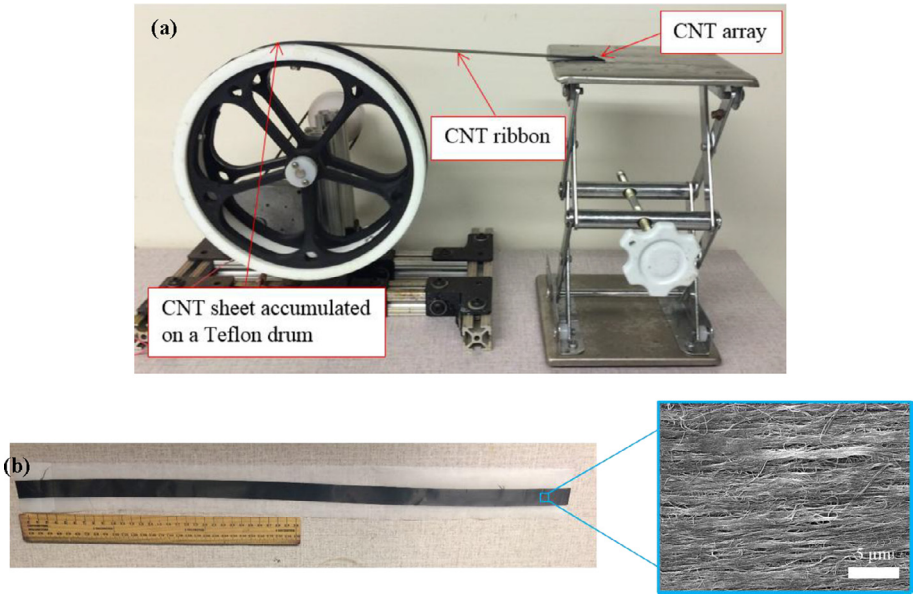

Fig. 1. (a) CNT ribbon being drawn from a CNT array and accumulated on a Teflon-covered drum to form a sheet and (b) CNT sheet after accumulation and densification, displayed along a 30-cm ruler. SEM image in the inset shows CNT alignment direction.

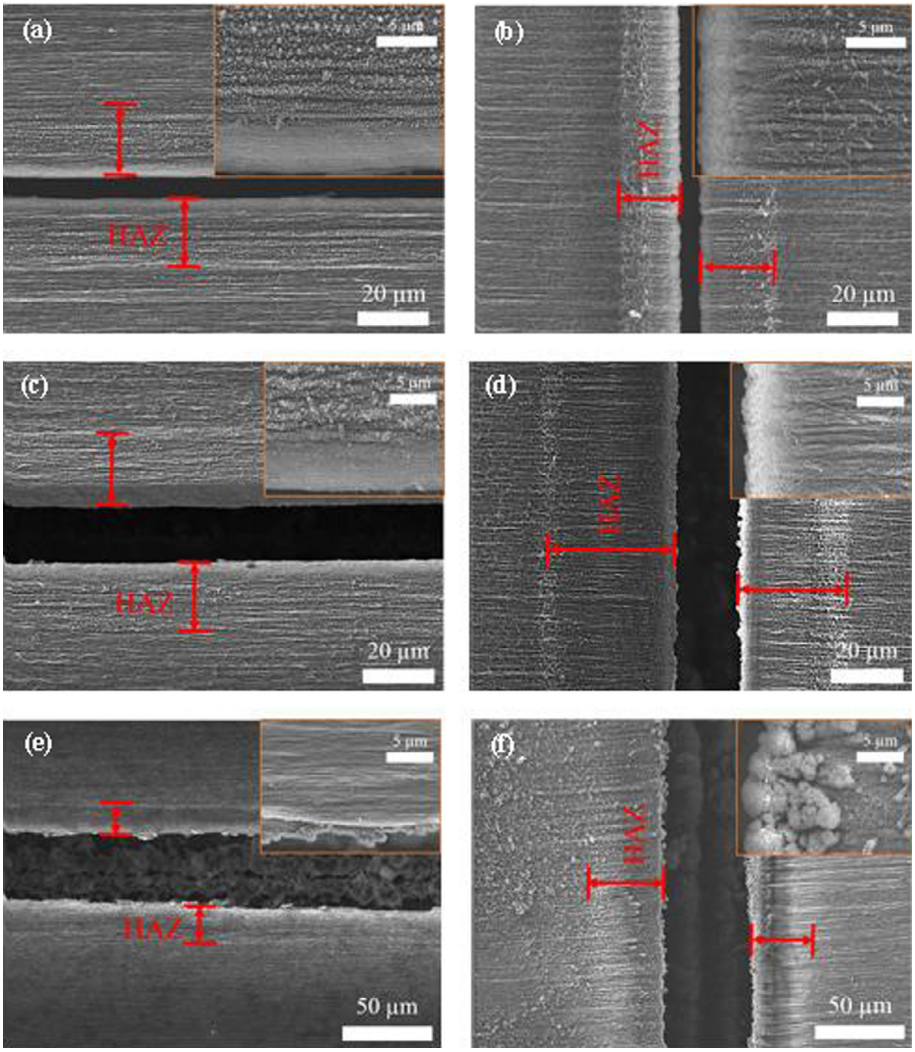

Fig. 2. SEM images of CNT sheets cut with laser powers of (a) 0.5%, (c) 5%, and (e) 50% in the parallel direction and (b) 0.5%, (d) 5%, and (f) 50% in the perpendicular direction to the nanotube alignment direction.

3. Results and discussion

3.1. Effects of laser power on the structure and morphology of CNT sheet

Different laser powers (0.5%, 5%, and 50% of the average power) were used to cut CNT sheets in the parallel and perpendicular directions to nanotube alignment. The effects of different laser powers on the kerf width (material removed) and HAZ were examined by SEM as shown in Fig. 2. The HAZ is marked in red on the SEM images and is distinguished by a change in appearance near the cut edge compared to the rest of the CNT sheet. Three different samples for each power level were prepared to measure the HAZ and kerf width. Multiple (8) HAZ and kerf width measurements were taken on these samples, and the average values are presented in Table 1.

Results reported reveal that increasing the laser power led to an increase in the kerf width in both parallel and perpendicular directions. The average HAZ and kerf width of CNT sheets cut in parallel and perpendicular directions to nanotube alignment using 0.5% laser power did not show much difference. The kerf width showed a slight increase in the perpendicular direction compared to that in the parallel direction for sheets cut using 5% and 50% laser power. The HAZ at these power levels also revealed a similar trend. This indicates that the laser power has an effect on both the HAZ and kerf of CNT sheets. The cross-sectional areas of the cut samples were also analyzed, and the obtained results are presented in Fig. 3 including a control sample that was cut with a scalpel. Laser damage can be clearly seen on the laser cut samples compared to that on the sample cut with a scalpel, as shown in Fig. 3(d).

Further investigations of the damage caused by laser cutting on CNT sheets were performed by running Raman spectroscopy on samples cut in the parallel and perpendicular directions. As an

Table 1
Average kerf width and HAZ of laser cut sheets in the parallel and perpendicular directions to the drawing direction.

Laser Power (Direction)	Kerf width (μm)	HAZ (μm)
0.5% (parallel)	6.2 ± 0.7	21.1 ± 1.2
0.5% (perpendicular)	6.3 ± 0.7	20.4 ± 2.2
5% (parallel)	15.5 ± 0.7	20.4 ± 1.8
5% (perpendicular)	19.4 ± 1.6	30.4 ± 5.4
50% (parallel)	44.2 ± 4.4	22.0 ± 3.4
50% (perpendicular)	49.4 ± 2.6	38.9 ± 3.6

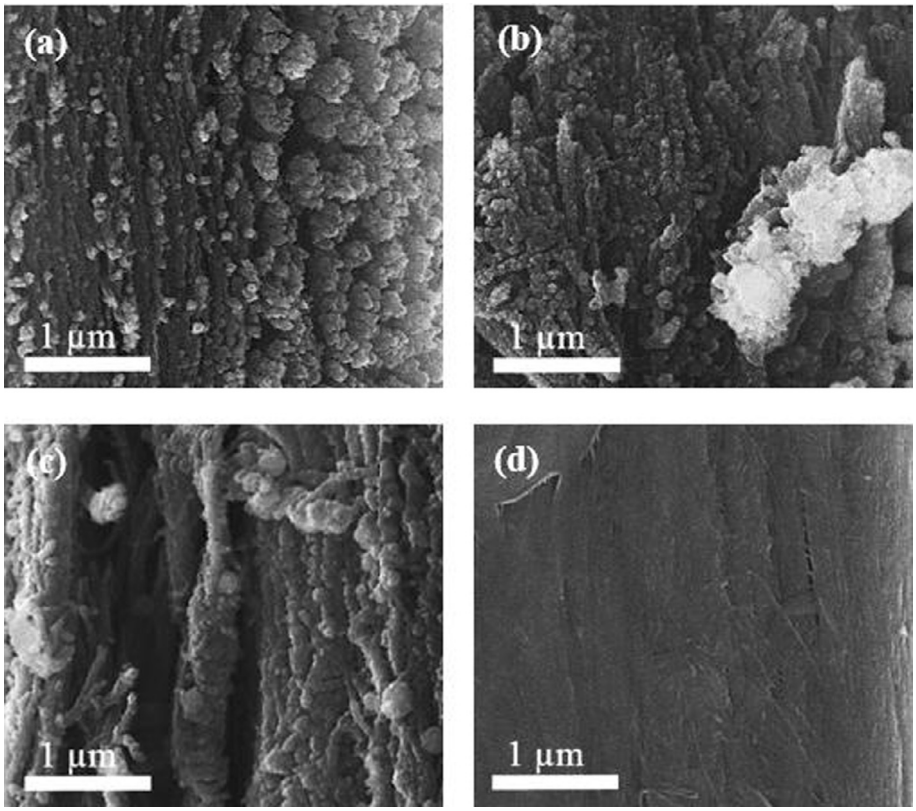

Fig. 3. Cross-sectional SEM images of samples cut at (a) 0.5% laser power, (b) 5% laser power, and (c) 50% laser power and (d) the sample cut by a scalpel.

example, samples cut with the lowest power (0.5%) were examined. The samples were mounted on a silicon substrate for Raman analysis. Fig. 4 shows the Raman spectra at 5, 10, 30, and 70 μm off the cut edge. There were two main peaks notably the D band and G band located at 1335 and 1583 cm^{-1}, respectively. The D band, also known as the disorder mode, can be attributed to the occurrence of disorder in carbon systems, while the G band can be attributed to the in-plane vibration of the C-C bond [33–35]. A deconvolution of

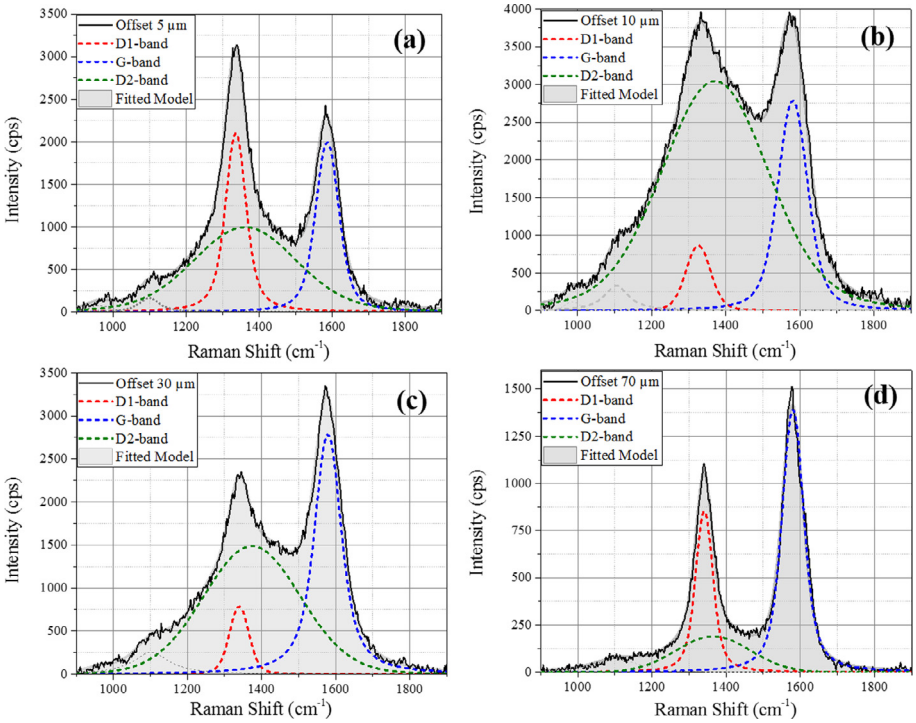

Fig. 4. Raman spectra of CNT sheets cut with 0.5% laser at (a) 5, (b) 10, (c) 30, and (d) 70 μm off the laser cut edge.

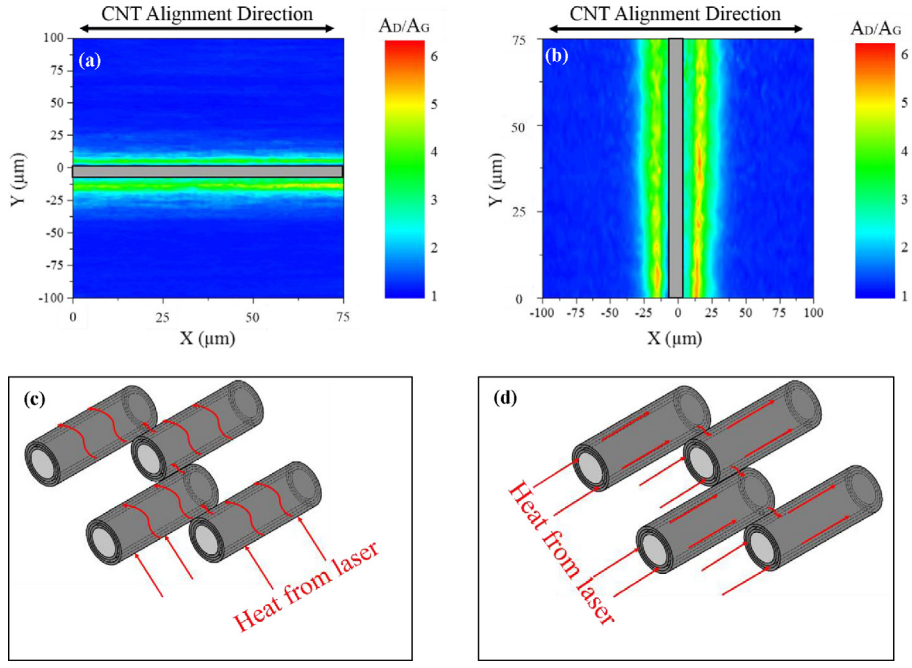

Fig. 5. Raman spectral mapping for CNT sheet cut with 0.5% laser power in (a) parallel and (b) perpendicular directions of nanotube alignment with kerf width indicated by the gray area. A schematic illustration of heat transfer from laser: (c) across nanotubes and (d) along nanotubes.

these bands showed two peaks for the D band, noted here as D1 and D2 located at 1337 and 1367 cm^{-1}, respectively. There are two other peaks at 1097 and 967 cm^{-1} belonging to the substrate. It is seen that at 5 μm off the edge, the D band was higher than the G band, which is suggestive of defects in the CNTs. However, at 10 μm off the edge, the D band broadened as well, even though there was a decrease in the intensity. The broadening of the D band is indicative of an increase in the disorder of the CNTs, leading us to believe that there might be an amorphization of CNTs at this point [36]. Further at 30 and 70 μm off the edge, an additional decrease

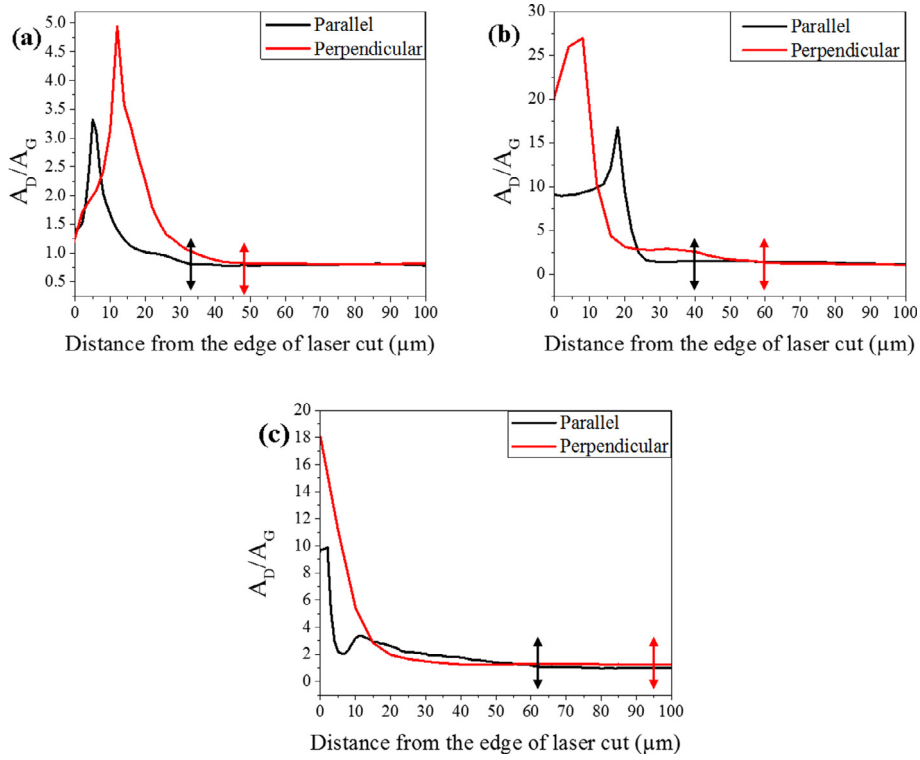

Fig. 6. Raman profiles tracked from the cut edge up to 100 μm into the CNT sheet for samples cut with (a) 0.5%, (b) 5%, and (c) 50% laser powers in both parallel and perpendicular directions.

in the D band and an increase in the G band were found, indicating less damage to the nanotubes, as determined by Raman spectroscopy.

On the basis of this analysis, a 200 × 75 μm area was scanned (2D Raman spectroscopy) at a 2 s/point acquisition time, and a total of 15,000 spectra were collected. The areas under the curves for D1, D2, and G were analyzed to get the degree of defects of CNTs. The ratio of the D band to the G band areas (A_D/A_G) was studied, where the D band area was calculated from the addition of D1 and D2 curves. This ratio was applied to the scanned area to get Raman spectral maps for parallel and perpendicular cut directions and are presented in Fig. 5(a) and (b), respectively. A_D/A_G for CNTs in areas not affected by the laser cutting was 0.68, and this increased as the defect concentration elevated. It can be seen from Fig. 5(a) and (b) that the damage done by the laser was not only limited to the cut edge but also spread well into the sheet. This reveals that the damage done on CNT sheets goes further than the HAZ visible by SEM analysis. The damage was also more pronounced in sheets cut in the perpendicular direction than that in those cut in the parallel direction. This difference in damage was a result of the differing modes of heat transfer or dissipation through the nanotubes, as illustrated in Fig. 5 (c) and (d). We assume that the temperature in the cutting zone (focal spot) can exceed 1000 °C for the duration of the pulse [37]. The generated heat is transferred better along the tubes (which is the case for sheets cut in the perpendicular direction), leading to a proliferation of damage, than that across the tubes (which is the case for sheets cut in the parallel direction). This is a result of the presence of more interfaces between successive tubes that leads to increased thermal resistance for heat transmitted across the tubes. However, the main mechanism for heat transfer along the tubes is through the length of the tube, which offers little

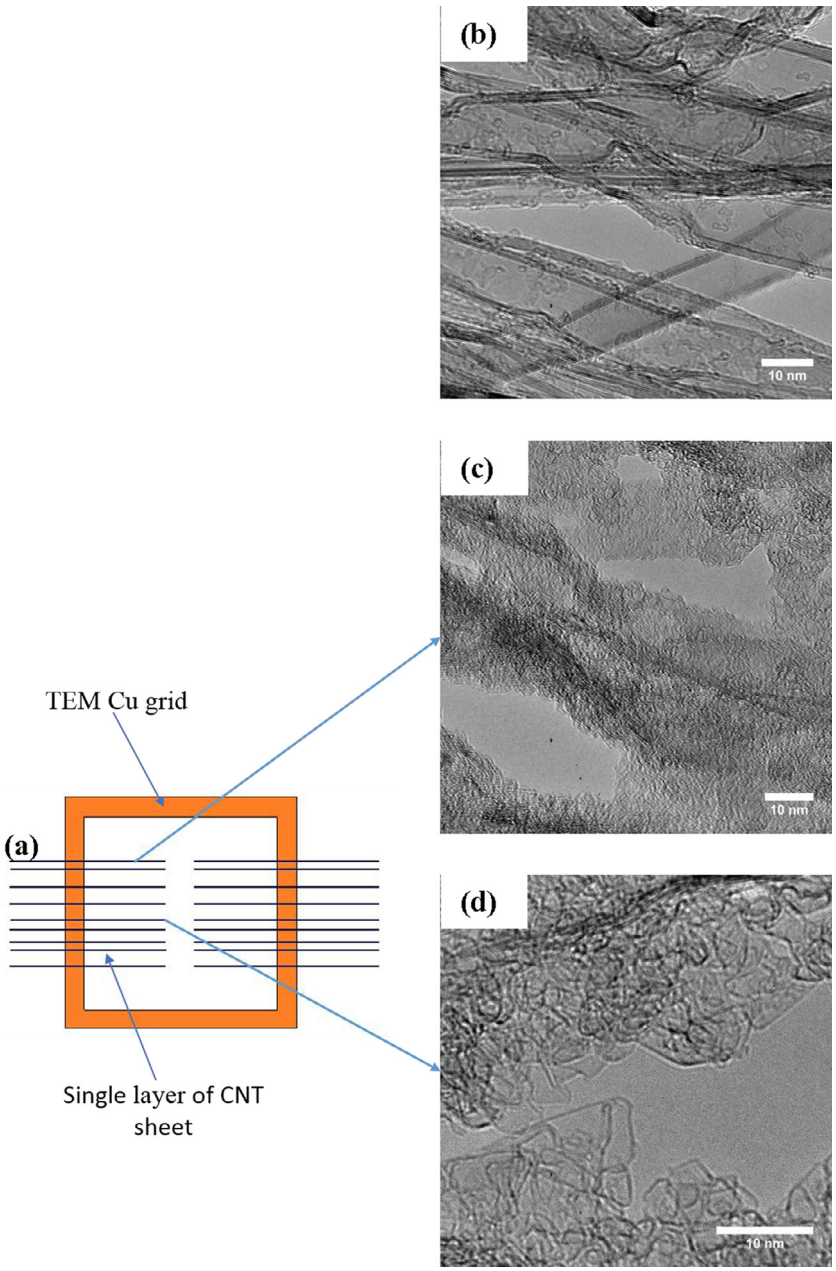

Fig. 7. (a) Schematic representation of aligned CNT bundles on a TEM grid and TEM images showing (b) bundles not exposed to laser CNTs, (c) laser damage of CNT bundles close to cut edge, and (d) laser damage of CNT bundles at the cut edge.

thermal resistance. Ali et al. reported a 23 times increase in thermal conductivity along the nanotube bundles compared to the direction across the aligned MWCNT sheet [38]. The thermal conductivity of CNT sheets fabricated by our group was as low as 2.5 W/m.K for a CNT sheet along the nanotubes at room temperature [39], and thus, a lower thermal conductivity was expected across the nanotube bundles. The difference in thermal conductivity explains why there was more thermal damage for the CNT sheet cut perpendicular to the CNT alignment direction than that for that cut parallel to the alignment direction. Raman profiles were also run across the cut sheets from the edge up to 100 μm into the sheet for sheets cut with 0.5%, 5%, and 50% laser powers and are presented in Fig. 6. It can be seen that as the laser power was increased from 0.5% to 5%, there was an increase in the defect-indicating ratio A_D/A_G. However, the ratio at 50% was less than that at 5%. This is because the high power laser (50%) cut the CNT sheet in the first pass, and therefore, subsequent second and third passes did not interact with the CNTs as much as that of the first. For 5% laser power, it took three passes to completely cut the sheet, and therefore, this increased the thermal damage during each pass. It is also seen that for each cut sample perpendicular to the tubes' direction, the defect-indicating ratio, A_D/A_G, for the perpendicular cut was always higher than that for the parallel cut. This is due to the difference in thermal conductivity, which depends on the tube orientation, as explained before. The HAZ was measured on the Raman profile graphs from the cut edge (distance = 0 μm) to the point where the ratio drops to that of a pristine material. The end of the HAZ related to different directions is marked by red and black arrows for parallel and perpendicular cuts, respectively. It can be seen that the HAZ determined by Raman spectroscopy is greater than that determined by SEM. This indicates that the thermal damage done on the sheets is more pronounced than that revealed by normal visual techniques commonly used to measure HAZ.

To elucidate the kind of damage that individual nanotubes undergo, TEM was used to study the structure of CNTs cut with a 0.5% laser power. Fig. 7 shows the TEM images of a single layer (ribbon) of CNT sheet cut with a laser and those of nondamaged CNTs. Because the sample has to be almost transparent for TEM

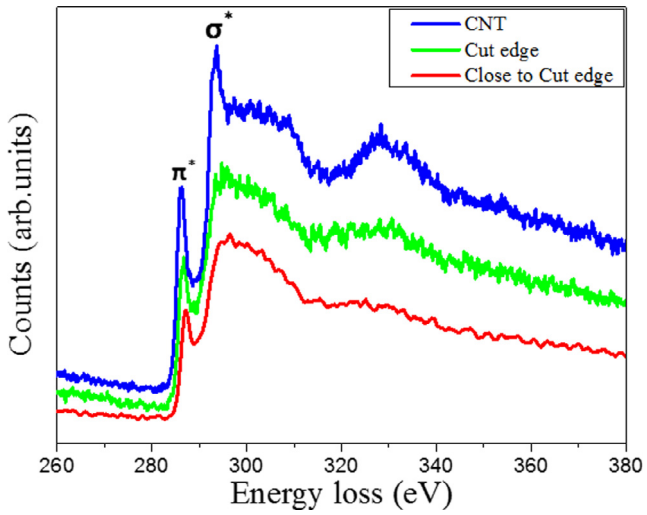

Fig. 8. Core loss EELS of nondamaged CNTs, laser damaged CNTs at the cut edge; and CNTs in an area close to the cut edge.

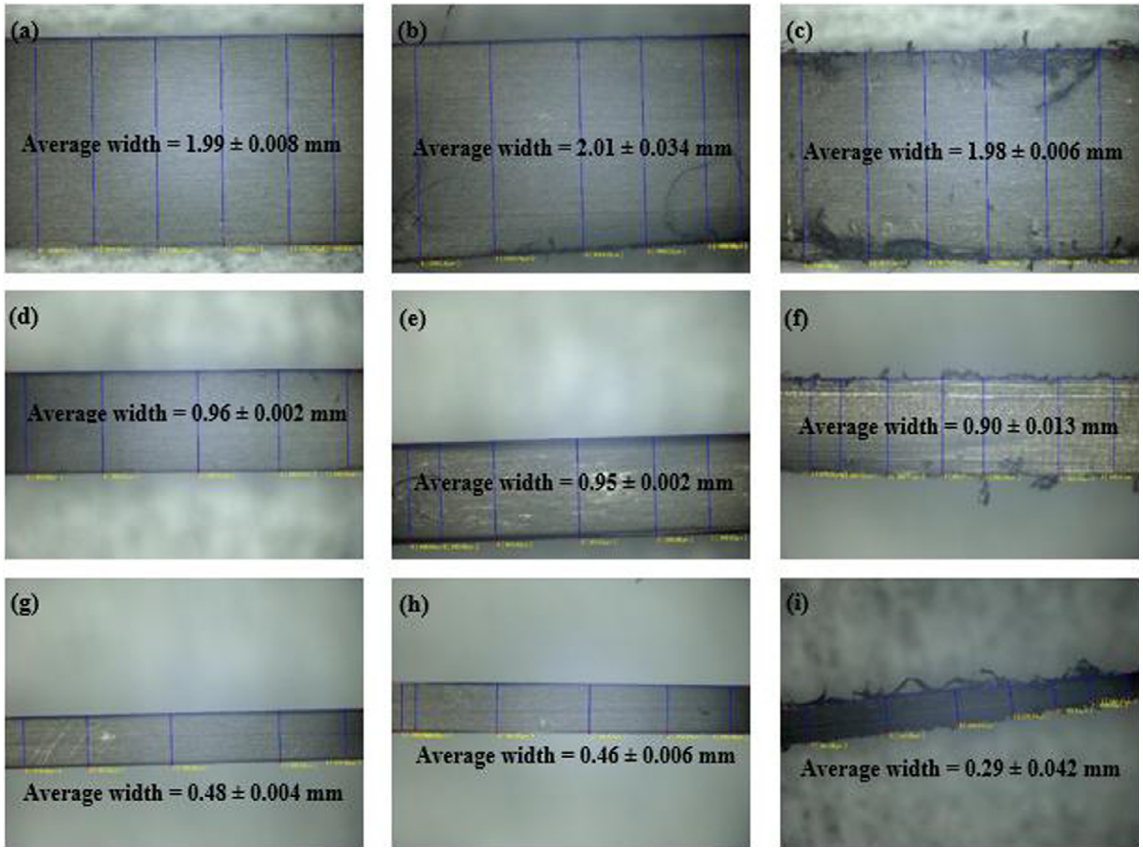

Fig. 9. Optical images at 100× magnification of laser cut samples at (a) 0.5% power, (b) 5% power, (c) 50% power to a sample's width of 2 mm, (d) 0.5% power, (e) 5% power, (f) 50% power to a sample's width of 1 mm, (g) 0.5% power, (h) 5% power, and (i) 50% power to a sample's width of 0.5 mm.

analysis, a single layer of CNT sheet was prepared and mounted on a Cu grid, as shown in the schematic in Fig. 7(a). The authors are aware that the overall heat transfer through a single layer of CNT sheet is different from a 100-layer sheet and this is discussed herein. Zhang et al. showed that the thermal conductivity of a MWCNT sheet (film) with a thickness between 10 and 50 μm is around 15 W/m.K at room temperature [40]. However, when they considered the volume filling fraction, they reported an effective nanotube thermal conductivity of around 200 W/m.K. This makes us believe that the heat conducted and dissipated by a single CNT layer would be different from what is dissipated by a bulk multilayer sheet. Nevertheless, this study may help understand the damage that laser cutting can impose on individual nanotubes. It can be seen from the TEM images that the CNT bundles not exposed to any laser damage (Fig. 7(b)) were completely different from those exposed to laser damage, as shown in Fig. 7(c) and (d). There is also a variation between the structure of CNTs close (~1 μm) to the cut edge (Fig. 7(c)) and that at the cut edge (Fig. 7 (d)). The area closest to the cut edge and the area at the cut edge reveal structures that are less crystalline than the area not exposed to the laser beam. Additional analysis was conducted to study this phenomenon by EELS. Core loss EELS spectra were collected by TEM at three different spots of interest on the sheet, and the results are presented in Fig. 8. A transition of a 1s electron to the π* antibonding orbital is shown by the feature at 285 eV. A second prominent feature occurs at around 295 eV and is representative of excitations to σ* states. An EELS spectrum gives information about the type of bonding (sp^2 or sp^3) that is present within the studied spot. Graphitic structures are mostly sp^2 bonded [41], while amorphous carbon is a mixture of sp^2 and sp^3 bonding [42]. Knowing the intensity ratio and features of σ* and π* bonds, one can determine what carbon structure is present within the EELS studied spot. The EELS spectrum of the damaged CNTs close to the cut edge is shown in red in Fig. 8.

This type of spectrum is observed for amorphous carbon (glassy carbon) materials where the π* feature is sharp and defined and the σ* position is smooth and featureless [41,43]. The EELS spectrum at the cut edge is displayed in green and shows a slight increase in the π* feature and an emergence of the σ* feature. This spectrum is indicative of a highly disordered carbon structure [41]. The spectrum observed for nondamaged CNTs (shown in blue) is, however, more pronounced for a crystalline structure typical of graphitic materials, where an increase in the π* feature and a sharp σ* peak appear [44]. The EELS spectra results show that there is a

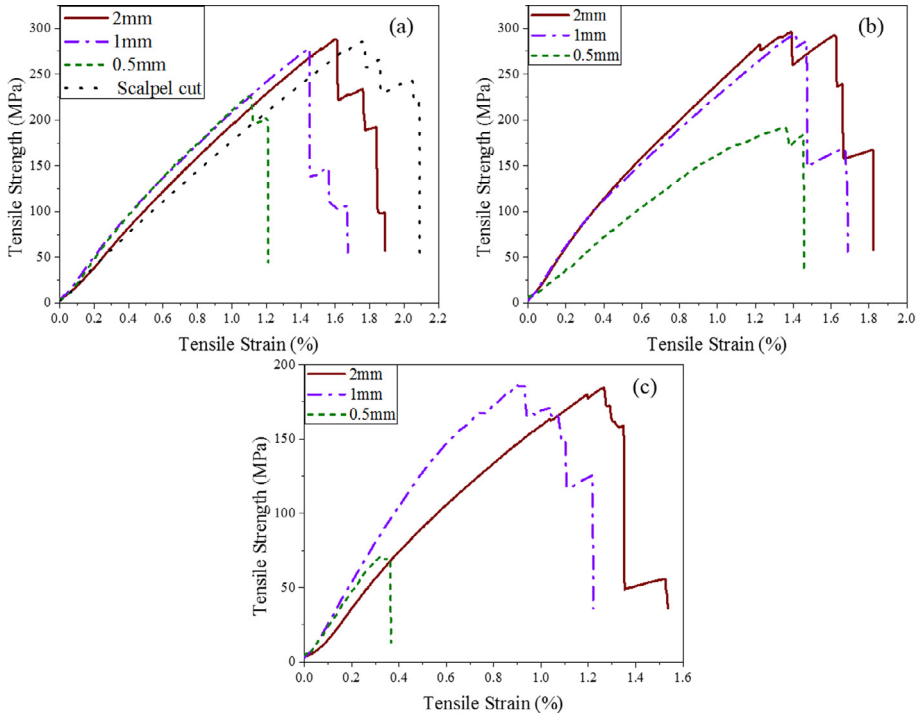

Fig. 10. Representative stress-strain curves for (a) 0.5%, (b) 5%, and (c) 50% laser power used to cut CNT sheets to different widths.

Table 2
Mechanical properties of CNT sheets cut to different widths at varying laser powers.

Width (mm)	Laser power (%)	Tensile Strength (MPa)	Young's Modulus (GPa)	Toughness (kJ/m^{-3})
2	Scalpel cut	272.15 ± 31.08	21.08 ± 3.46	3263.11 ± 281.36
2	0.5	295.98 ± 20.30	26.08 ± 3.83	3155.70 ± 259.81
	5	290.97 ± 26.46	27.58 ± 3.40	2845.63 ± 489.80
	50	164.68 ± 54.35	22.28 ± 5.82	1716.45 ± 732.74
1	0.5	277.16 ± 28.68	27.26 ± 3.58	2428.40 ± 294.11
	5	291.32 ± 55.44	30.03 ± 3.95	2589.65 ± 425.31
	50	154.05 ± 88.27	22.15 ± 7.02	1144.64 ± 728.39
0.5	0.5	237.71 ± 48.98	27.96 ± 6.78	1531.75 ± 604.10
	5	192.36 ± 68.40	24.86 ± 5.33	1219.06 ± 697.97
	50	59.67 ± 42.38	21.61 ± 6.03	104.22 ± 53.18

transformation of CNTs into a less-crystalline structure such as amorphous carbon during the laser cutting process.

3.2. Effects of laser cutting on mechanical properties of CNT sheets

The effect of laser cutting on the mechanical properties of CNT sheets was investigated by preparing samples of 40-mm length with three different widths (2, 1, and 0.5 mm). Ten test samples for each cut width were prepared with a gauge length of 22 mm for mechanical measurements. Samples were cut at 0.5%, 5%, and 50% power levels. Optical microscopy images of all cut samples obtained using a Keyence VHX 2000 instrument are presented in Fig. 9. CNT sheets cut with 50% laser power at different widths showed the most thermal damage as observed in Fig. 9(c), (f), and (i). There was also many fiber pullouts at the ends of sheets cut at this power level compared to sheets cut with 0.5% and 5% laser power. Representative stress-strain curves for CNT sheets obtained with 0.5%, 5%, and 50% laser power at different cut widths are displayed in Fig. 10.

A scalpel cut sample with a width and length of 2 mm and 40 mm respectively, was used as a control, and this is presented in Fig. 10(a). Stress-strain curves show a failure mechanism based on sliding of CNTs in the material typical of pristine CNT sheets [45]. CNTs slide and break leading to a decrease in the stress; however, because the total sample is not completely fractured, the sheet still supports some stress until complete failure. The mechanical properties are nevertheless expected to be the same for each sample width.

Table 2 presents the tensile strength, Young's modulus, and toughness results for tested sheets. It is observed that regardless of the final width of the CNT sheet, samples cut with 50% laser power had the least tensile strength and toughness. This is because the ends of the sheets were damaged (split) more extensively by the high-intensity laser power, as shown in Fig. 9(c), (f), and (i). Samples cut with 5% and 0.5% laser power had comparable tensile strength to the scalpel cut sample with 2- and 1-mm widths. The toughness of these sheets was, however, reduced at 1-mm cut width indicating an effect of the laser power at this dimension. However, for samples cut to a width of 0.5 mm, there was a reduction in tensile strength, toughness, and Young's modulus, and this is more drastic in the case of 50% laser power cut sample. There was a reduction in tensile strength by as much as 75% compared to the 0.5% laser power cut sample with the same width. This is due to the occurrence of tear out, extreme damage, and a reduction in the thickness (42%) of the sample as shown in Fig. 9(i). For samples cut to a width of 0.5 mm by 5% and 0.5% laser power, although the average width was not reduced as much as the 50% laser power cut sample, we believe the HAZ contributed to their lower mechanical properties. As discussed in the Raman analysis, the HAZ mostly consists of amorphous carbon, which does not have the same structural properties as those of pristine CNTs. This therefore reduces the amount of the pristine material contributing to the mechanical properties. The latter implies that there is a size threshold below which the laser cutting has a more pronounced effect on the mechanical properties, irrespective of the laser power used.

4. Conclusion

This study showed that the amount of laser power must be considered when cutting samples from CNT assemblages as it can have a profound impact on the material's properties. Laser cutting causes changes in the structural properties of CNTs at the cut edge. However, the damage done by the laser is not limited to the cut edge and spreads well into the sample. Samples cut with high laser power exhibited lower mechanical properties and defects. At lower cut widths though, samples cut with lower laser power demonstrated a reduction in the mechanical properties as well. Amorphous carbon formed by laser cutting may also affect other applications where the material's quality needs to be close to that of pristine CNTs.

Acknowledgment

This work was funded by the National Science Foundation (NSF) through the following grants: CMMI-0727250, SNM-1120382, and ERC-0812348. The authors also appreciate the financial support of DURIP-ONR N00014-15-1-2473, ARMY W911NF-16-2-0026, and NASA NNX13AF46A. SG is thankful for the graduate assistantship provided to him by the College of Engineering and Applied Science (CEAS) and for the ERC PRP grant at UC.

References

[1] L.V. Radushkevich, V.M. Lukyanovich, About the structure of carbon formed by thermal decomposition of carbon monoxide on iron substrate, J. Phys. Chem. 26 (1952) 88–95.
[2] L.J.E. Hofer, E. Sterling, J.T. McCartney, Carbon deposits from carbon monoxide on iron, cobalt and nickel, J. Phys. Chem. 59 (11) (1955) 1153–1155.
[3] S. Iijima, Helical microtubules of graphitic carbon, Nature 354 (6348) (1991) 56–58.
[4] A.A. Balandin, Thermal properties of graphene and nanostructured carbon materials, Nat. Mater. 10 (8) (2011) 569–581.
[5] R. Zhang, Q. Wen, W. Qian, D.S. Su, Q. Zhang, F. Wei, Superstrong ultralong carbon nanotubes for mechanical energy storage, Adv. Mater. 23 (30) (2011) 3387–3391.
[6] Q. Li, Y. Li, X. Zhang, S.B. Chikkannanavar, Y. Zhao, A.M. Dangelewicz, et al., Structure-dependent electrical properties of carbon nanotube fibers, Adv. Mater. 19 (20) (2007) 3358–3363.
[7] K. Jiang, J. Wang, Q. Li, L. Liu, C. Liu, S. Fan, Superaligned carbon nanotube arrays, films, and yarns: a road to applications, Adv. Mater. 23 (9) (2011) 1154–1161.
[8] C. Jayasinghe, S. Chakrabarti, M.J. Schulz, V. Shanov, Spinning yarn from long carbon nanotube arrays, J. Mater. Res. 26 (05) (2011) 645–651.
[9] Y.-L. Li, I.A. Kinloch, A.H. Windle, Direct spinning of carbon nanotube fibers from chemical vapor deposition synthesis, Science 304 (5668) (2004) 276–278.
[10] W. Li, C. Jayasinghe, V. Shanov, M. Schulz, Spinning carbon nanotube nanothread under a scanning electron microscope, Materials 4 (9) (2011) 1519–1527.
[11] K. Jiang, Q. Li, S. Fan, Nanotechnology: Spinning continuous carbon nanotube yarns, Nature 419 (6909) (2002). 801-801.
[12] M. Schulz, Y. Song, A. Hehr, V. Shanov, Embedded carbon nanotube thread piezoresistive strain sensor performance, Sens. Rev. 34 (2) (2014) 209–219.
[13] M. Zhang, S. Fang, A.A. Zakhidov, S.B. Lee, A.E. Aliev, C.D. Williams, et al., Strong, transparent, multifunctional, carbon nanotube sheets, Science 309 (5738) (2005) 1215–1219.
[14] R.H. Baughman, A.A. Zakhidov, W.A. de Heer, Carbon nanotubes–the route toward applications, Science 297 (5582) (2002) 787–792.
[15] A.B. Dalton, S. Collins, E. Muñoz, J.M. Razal, V.H. Ebron, J.P. Ferraris, et al., Super-tough carbon-nanotube fibres, Nature 423 (6941) (2003). 703-703.
[16] K. Liu, Y. Sun, L. Chen, C. Feng, X. Feng, K. Jiang, et al., Controlled growth of super-aligned carbon nanotube arrays for spinning continuous unidirectional sheets with tunable physical properties, Nano Lett. 8 (2) (2008) 700–705.
[17] F. Ren, S.A. Kanaan, F. Khalkhal, C.Z. Loebick, G.L. Haller, L.D. Pfefferle, Controlled cutting of single-walled carbon nanotubes and low temperature annealing, Carbon 63 (2013) 61–70.
[18] U. Rauwald, J. Shaver, D.A. Klosterman, Z. Chen, C. Silvera-Batista, H.K. Schmidt, et al., Electron-induced cutting of single-walled carbon nanotubes, Carbon 47 (1) (2009) 178–185.
[19] Z. Xu, L. Xu, F. Fang, H. Gao, W. Li, Carbon nanotube's modification by focused ion beam irradiation and its healing strategies, Nucl. Instrum. Methods Phys. Res., Sect. B 307 (2013) 203–206.
[20] G. Chai, L. Chow, D. Zhou, S.R. Byahut, Focused-ion-beam assisted fabrication of individual multiwall carbon nanotube field emitter, Carbon 43 (10) (2005) 2083–2087.
[21] J. Wu, M. Eastman, T. Gutu, M. Wyse, J. Jiao, S.-M. Kim, et al., Fabrication of carbon nanotube-based nanodevices using a combination technique of focused ion beam and plasma-enhanced chemical vapor deposition, Appl. Phys. Lett. 91 (17) (2007) 173122.
[22] K.Y. Lim, C.H. Sow, J. Lin, F.C. Cheong, Z.X. Shen, J.T.L. Thong, et al., Laser pruning of carbon nanotubes as a route to static and movable structures, Adv. Mater. 15 (4) (2003) 300–303.
[23] Y. Wei, P. Liu, F. Zhu, K. Jiang, Q. Li, S. Fan, Efficient fabrication of carbon nanotube micro tip arrays by tailoring cross-stacked carbon nanotube sheets, Nano Lett. 12 (4) (2012) 2071–2076.

[24] S.B. Fairchild, J.S. Bulmer, M. Sparkes, J. Boeckl, M. Cahay, T. Back, et al., Field emission from laser cut CNT fibers and films, J. Mater. Res. 29 (03) (2014) 392–402.
[25] N.T. Hong, I.H. Baek, F. Rotermund, K.H. Koh, S. Lee, Femtosecond laser machining: a new technique to fabricate carbon nanotube based emitters, J. Vac. Sci. Technol., B 28 (2) (2010). C2B38-C2B42.
[26] A. Karimzad Ghavidel, T. Azdast, M.R. Shabgard, A. Navidfar, S. Mamaghani Shishavan, Effect of carbon nanotubes on laser cutting of multi-walled carbon nanotubes/poly methyl methacrylate nanocomposites, Opt. Laser Technol. 67 (2015) 119–124.
[27] K.E. Hix, M. Li, J. Gosciniak, K. Hartke, M. Rendina, L.R. Dosser, et al., Femtosecond and nanosecond laser micromachining of oxidized multi-wall carbon nanotube doped morthane, in: Lasers and Applications in Science and Engineering, International Society for Optics and Photonics, 2005.
[28] F. Al-Sulaiman, B. Yilbas, M. Ahsan, CO 2 laser cutting of a carbon/carbon multi-lamelled plain-weave structure, J. Mater. Process. Technol. 173 (3) (2006) 345–351.
[29] M. Tachibana, Characterization of Laser-Induced Defects and Modification in Carbon Nanotubes by Raman Spectroscopy, INTECH Open Access Publisher, 2013.
[30] F.C. Cheong, K.Y. Lim, C.H. Sow, J. Lin, C.K. Ong, Large area patterned arrays of aligned carbon nanotubes via laser trimming, Nanotechnology 14 (4) (2003) 433.
[31] A. Karimzad Ghavidel, A. Navidfar, M. Shabgard, T. Azdast, Role of CO2 laser cutting conditions on anisotropic properties of nanocomposite contain carbon nanotubes, J. Laser Appl. 28 (3) (2016) 032006.
[32] N.T. Alvarez, P. Miller, M. Haase, N. Kienzle, L. Zhang, M.J. Schulz, et al., Carbon nanotube assembly at near-industrial natural-fiber spinning rates, Carbon 86 (2015) 350–357.
[33] L. Bokobza, J. Zhang, Raman spectroscopic characterization of multiwall carbon nanotubes and of composites, Express Polym. Lett. 6 (7) (2012) 601–608.
[34] H. Hiura, T. Ebbesen, K. Tanigaki, H. Takahashi, Raman studies of carbon nanotubes, Chem. Phys. Lett. 202 (6) (1993) 509–512.
[35] Y. Wang, D.C. Alsmeyer, R.L. McCreery, Raman spectroscopy of carbon materials: structural basis of observed spectra, Chem. Mater. 2 (5) (1990) 557–563.
[36] M. Dresselhaus, A. Jorio, A. Souza Filho, R. Saito, Defect characterization in graphene and carbon nanotubes using Raman spectroscopy, Philos. Trans. R. Soc. Lond. A: Math. Phys. Eng. Sci. 368 (1932) (2010) 5355–5377.
[37] L. Torrisi, F. Caridi, D. Margarone, A. Picciotto, A. Mangione, J. Beltrano, Carbon-plasma produced in vacuum by 532 nm–3 ns laser pulses ablation, Appl. Surf. Sci. 252 (18) (2006) 6383–6389.
[38] E.A. Ali, H.L. Marcio, M.S. Edward, H.B. Ray, Thermal conductivity of multi-walled carbon nanotube sheets: radiation losses and quenching of phonon modes, Nanotechnology 21 (3) (2010) 035709.
[39] J.-H. Pöhls, M.B. Johnson, M.A. White, R. Malik, B. Ruff, C. Jayasinghe, et al., Physical properties of carbon nanotube sheets drawn from nanotube arrays, Carbon 50 (11) (2012) 4175–4183.
[40] Q. Zhang, G. Chen, S. Yoon, J. Ahn, S. Wang, Q. Zhou, et al., Thermal conductivity of multiwalled carbon nanotubes, Phys. Rev. B 66 (16) (2002) 165440.
[41] H. Daniels, R. Brydson, B. Rand, A. Brown, Investigating carbonization and graphitization using electron energy loss spectroscopy (EELS) in the transmission electron microscope (TEM), Philos. Mag. 87 (27) (2007) 4073–4092.
[42] R. Jarman, G. Ray, R. Standley, G. Zajac, Determination of bonding in amorphous carbon films: a quantitative comparison of core-electron energy-loss spectroscopy and 13C nuclear magnetic resonance spectroscopy, Appl. Phys. Lett. 49 (17) (1986) 1065–1067.
[43] J. Yuan, L.M. Brown, Investigation of atomic structures of diamond-like amorphous carbon by electron energy loss spectroscopy, Micron 31 (5) (2000) 515–525.
[44] K. Yase, S. Horiuchi, M. Kyotani, M. Yumura, K. Uchida, S. Ohshima, et al., Angular-resolved EELS of a carbon nanotube, Thin Solid Films 273 (1) (1996) 222–224.
[45] R. Malik, C. McConnell, N.T. Alvarez, M. Haase, S. Gbordzoe, V. Shanov, Rapid, in situ plasma functionalization of carbon nanotubes for improved CNT/epoxy composites, RSC Adv. 6 (110) (2016) 108840–108850.